Neurobiology of Disease 134 (2020) 104675

Contents lists available at ScienceDirect

Neurobiology of Disease

journal homepage: www.elsevier.com/locate/ynbdi

Laquinimod ameliorates secondary brain inflammation

Julia Nedelcu[a,b], Christin Reinbach[a,b], Philipp Riedler[a,b], Matthias Brendel[c], Axel Rominger[d], Joel Kaye[e], Newshan Behrangi[a], Zhan Jiangshan[a], Christoph Schmitz[b], Markus Kipp[a,*]

[a] Institute of Anatomy, Rostock University Medical Center, Rostock 18057, Germany
[b] Department of Anatomy II, Ludwig-Maximilians-University of Munich, Munich 80336, Germany
[c] Department of Nuclear Medicine, University Hospital, LMU Munich, Munich 80336, Germany
[d] Department of Nuclear Medicine, Inselspital, University Hospital Bern, Bern, Switzerland
[e] AyalaPharma, VP Research & Nonclinical Development, Rehovot, Israel

ARTICLE INFO

Keywords:
Cuprizone
Laquinimod
Demyelination
Multiple sclerosis

ABSTRACT

Accumulating evidence suggests that a degenerative processes within the brain can trigger the formation of new, focal inflammatory lesions in Multiple Sclerosis (MS). Here, we used a novel pre-clinical MS animal model to test whether the amelioration of degenerative brain events reduces the secondary recruitment of peripheral immune cells and, in consequence, inflammatory lesion development.

Neural degeneration was induced by a 3 weeks cuprizone intoxication period. To mitigate the cuprizone-induced pathology, animals were treated with Laquinimod (25 mg/kg) during the cuprizone-intoxication period. At the beginning of week 6, encephalitogenic T cell development in peripheral lymphoid organs was induced by the immunization with myelin oligodendrocyte glycoprotein 35–55 peptide (i.e., Cup/EAE). Demyelination, axonal injury and reactive gliosis were determined by immunohistochemistry. Positron emission tomography (PET) imaging was performed to analyze glia activation in vivo.

Vehicle-treated cuprizone mice displayed extensive callosal demyelination, glia activation and enhanced TSPO-ligand binding. This cuprizone-induced pathology was profoundly ameliorated in mice treated with Laquinimod. In vehicle-treated Cup/EAE mice, the cuprizone-induced pathology triggered massive peripheral immune cell recruitment into the forebrain, evidenced by multifocal perivascular inflammation, glia activation and neuro-axonal injury. While anti myelin oligodendrocyte glycoprotein 35–55 peptide immune responses were comparable in vehicle- and Laquinimod-treated Cup/EAE mice, the cuprizone-triggered immune cell recruitment was ameliorated by the Laquinimod treatment.

This study clearly illustrates that amelioration of a primary brain-intrinsic degenerative process secondary halts peripheral immune cell recruitment and, in consequence, inflammatory lesion development. These findings have important consequences for the interpretation of the results of clinical studies.

1. Introduction

Multiple sclerosis (MS) is a chronic inflammatory demyelinating disease of the central nervous system (CNS) causing disability in > 2.5 million people worldwide. On the histopathological level, brains of MS patients show perivascular inflammation, peripheral immune cell recruitment, demyelination, glia activation and axonal injury. Of note, the demyelination is not restricted to the white matter but can as well be found in the cortical and subcortical grey matter areas (Di Filippo et al., 2018; Kipp et al., 2012; Schmierer et al., 2018). Besides such focal lesions, diffuse tissue injury is characteristic for the MS brain. Diffuse tissue injuries in non-lesion containing brain areas has been demonstrated by various techniques including gene expression analyses, in situ hybridization, immunofluorescence studies (Aboul-Enein et al., 2003; Zeis et al., 2008), or by different imaging modalities such as proton magnetic resonance spectroscopic imaging (Fu et al., 1998) or Gadolinium enhanced magnetic resonance imaging (Silver et al., 2001). Since such areas of diffuse tissue injury do not show the 'classical demyelination' such affected areas are called 'normal appearing white and grey matter'. Clinically, MS can be categorized into three main groups: relapsing-remitting, secondary progressive, and primary progressive. While the pathological substrate of relapses is the focal, inflammatory demyelination, irreversible disease progression is due to neuroaxonal damage (i.e., neurodegeneration). Despite the availability of a number

* Corresponding author at: Rostock, Rostock University Medical Center, Institute of Anatomy, Gertrudenstrasse 9, 18056, Germany.
E-mail address: markus.kipp@med.uni-rostock.de (M. Kipp).

https://doi.org/10.1016/j.nbd.2019.104675
Received 11 July 2019; Received in revised form 21 October 2019; Accepted 11 November 2019
Available online 13 November 2019

Table 1
List of the primary antibodies used in this study.

Antigen	Species	Dilution	HIER method	Purchase number	RRID	Supplier
IBA1	rabbit	1:5000	Tris/EDTA	019-19741	AB_839504	Wako, USA
MAC3	rat	1:200	Tris/EDTA	550292	AB_393587	BD Pharmingen
Vimentin	rabbit	1:200	Tris/EDTA	ab92547	AB_10562134	Abcam, UK
GFAP	chicken	1:8000	Citrate	ab4674	AB_304558	Abcam, UK
ALDH1L1	rabbit	1:1000	None	ab87117	AB_10712968	Abcam, Uk
CD4	rabbit	1:1000	Tris/EDTA	ab183685	AB_2686917	Abcam, UK
APP	mouse	1:5000	Tris/EDTA	MAB348	AB_94882	Millipore, USA
VGluT1	mouse	1:1000	Citrate	ab134283	not available	Abcam, UK
Synaptophysin	mouse	1:300	Citrate	ab8049	AB_2198854	Abcam, UK

Table 2
List of the secondary antibodies used in this study.

	Dilution	Order number	RRID	Supplier
Goat anti-rabbit IgG	1:200	BA-1000	AB_2313606	Vector Laboratories, Burlingame, USA
Goat anti-rat IgG	1:200	BA-9400	AB_2336202	Vector Laboratories, Burlingame, USA
Goat anti-chicken IgG	1:200	BA-9010	AB_2336114	Vector Laboratories, Burlingame, USA
Goat anti-mouse IgG	1:200	BA-9200	AB_2336171	Vector Laboratories, Burlingame, USA
HRP-linked goat anti-mouse IgG	1:1	K4001	not available	Dako, Santa Clara, USA

of immunomodulatory drugs, which are mostly effective during the relapsing-remitting disease phase, there are no entirely satisfactory treatment options for secondary progressive and primary progressive MS patients.

Laquinimod, formerly called ABR-215062, is a small molecule developed as an orally available disease modifying treatment option in MS. This drug inhibits the development of disease in inflammatory mouse models for MS, such as experimental autoimmune encephalomyelitis (EAE) and experimental autoimmune neuritis (Thone et al., 2012; Yang et al., 2004; Zou et al., 2002). Laquinimod was equally protective in non-inflammatory CNS-disease models such as the cuprizone model (Bruck et al., 2012; Kramann et al., 2016), models of Huntigton disease (Ellrichmann et al., 2017; Garcia-Miralles et al., 2019) or traumatic brain injury (Katsumoto et al., 2018). Beyond, it has been shown that Laquinimod can regulate synaptic transmission by increasing inhibitory GABAergic post-synaptic currents, can reduce glutamatergic excitatory post-synaptic currents (Ruffini et al., 2013), and improve axonal remyelination and integrity in EAE (Moore et al., 2013). These and other findings suggest immunomodulatory, neuroprotective and neurorestorative effects of Laquinimod. Two independent clinical studies demonstrated that Laquinimod is effective in suppressing the development of active lesions in relapsing-remitting MS (Comi et al., 2008; Polman et al., 2005). With respect to its neuroprotective function, two subsequent placebo-controlled studies in relapsing-remitting MS showed significant reductions in brain atrophy by Laquinimod versus placebo (Comi et al., 2012; Vollmer et al., 2014). Evidence for a direct neuroprotective effect was as well reported in a follow-up imaging study (Filippi et al., 2014). Taken together, it is likely that Laquinimod combines anti-inflammatory and neuroprotective properties.

One major drawback for translational MS research is what we call the “clinical-preclinical discrepancy”. Inflammatory activity and CNS atrophy is, during most clinical studies, analyzed in the brain (i.e., in the forebrain/prosencephalon, the midbrain/mesencephalon and the hindbrain/rhombencephalon). In contrast, in classical EAE models (i.e., $MOG_{35–55}$-induced EAE in C57BL/6 mice) inflammatory lesions predominantly develop within the spinal cord and cerebellum, whereas other parts of the CNS are by far less severely affected. A model showing robust inflammatory lesion development in the forebrain would, thus, be valuable to study MS related pathologies and treatment effects. Our group and others recently demonstrated that primary oligodendrocyte degeneration, induced by cuprizone intoxication, can trigger peripheral immune cell recruitment into the forebrain after $MOG_{35–55}$ immunization (Baxi et al., 2015; Boretius et al., 2012; Ruther et al., 2017; Scheld et al., 2016). In the Scheld study, forebrain oligodendrocyte apoptosis was first induced by a 3-week intoxication with cuprizone, followed by the induction of encephalitogenic T-cell formation in peripheral lymphoid organs via the immunization with the myelin oligodendrocyte glycoprotein 35–55 peptide ($MOG_{35–55}$ + CFA/PTX; i.e., the induction of active EAE) at the beginning of week 6. This innovative model provides an excellent tool to study inflammatory lesion development and progression within the forebrain of mice. Furthermore, it allows to investigate the cell-cell communication pathways operant during CNS-triggered immune cell recruitment.

During the current study we, first, aimed to analyze whether Laquinimod ameliorates cuprizone-induced demyelination. Second, we were interested whether the Laquinimod-mediated amelioration of cuprizone-induced pathologies reduces the secondary recruitment of peripheral immune cells into the forebrain and, in consequence, inflammatory lesion development.

2. Material and methods

2.1. Animals and experimental groups

C57BL/6 female mice at 8 wks of age were obtained from Janvier Labs, Le Genest-Saint-Isle, France. All experimental procedures were approved by the Review Board for the Care of Animal Subjects of the district government (Regierung Oberbayern; reference number 55.2-154-2532-73-15; Germany). A maximum of five animals were housed per cage (435 cm^2). Animals were kept under standard laboratory conditions (12 h light/dark cycle, controlled temperature 23 °C ± 2 °C and 50% ± 5% humidity) with access to food and water ad libitum. The mice were allowed to accommodate to the environment for at least one week prior to the beginning of the experiments and were provided with nestlets for environmental enrichment. Body weights of mice were controlled once per week. The mice were randomly assigned to the experimental groups as illustrated in supplementary Fig. 1. (A) Control, animals were provided a diet of standard rodent chow for the entire duration of the study. (B) Cup/Vehicle, the animals were intoxicated with a diet containing 0.25% cuprizone for three weeks, followed by two weeks of normal chow. A vehicle solution was administered daily by oral gavage (200 µl) during week 1–3. (C) Cup/Laquinimod, the animals were intoxicated with a diet containing 0.25% cuprizone for

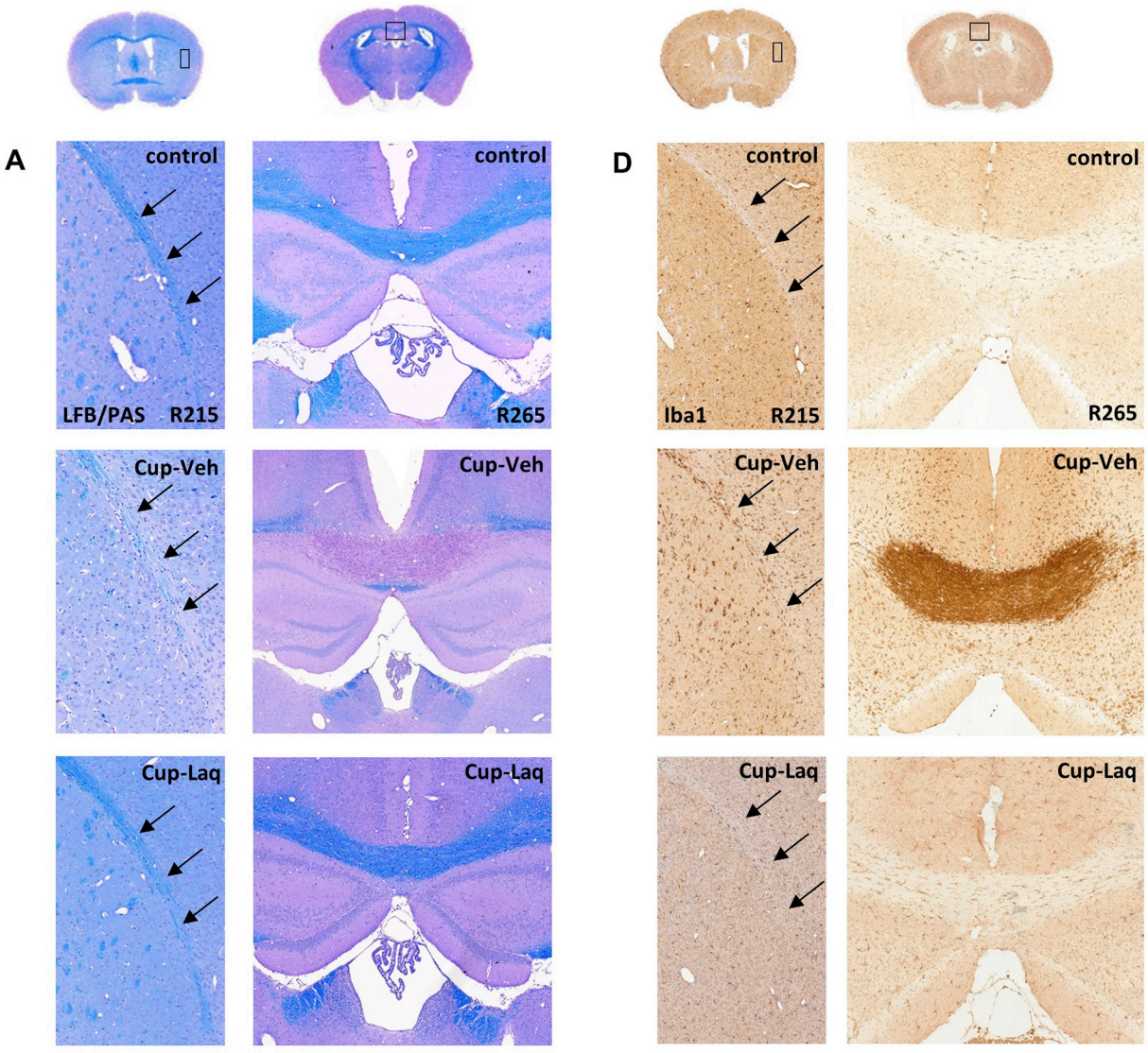

(caption on next page)

Fig. 1. Laquinimod ameliorates cuprizone-induced demyelination and microgliosis.
(A) Representative LFB/PAS stains of the lateral CC (region 215; left) and midline of the CC (region 265; right). Arrows highlight the lateral part of the CC in region 215. (B/C) Extent of demyelination, determined in LFB/PAS stained sections (R215 in B and R265 in C; control: $n = 5$, Cup-Veh: $n = 10$, Cup-Laq: n = 10). Differences were determined using Kruskal-Wallis-Test, followed by Dunn's multiple comparisons test. (D) Representative anti-IBA1 stained sections of the lateral CC (region 215; left) and midline of the CC (region 265; right). Arrows highlight the lateral part of the CC in region 215. (E/F) Extent of microglia/monocyte reactivity, determined in IBA1-stained sections (R215 in E and R265 in F; control: n = 5, Cup-Veh: n = 10, Cup-Laq: n = 10). Differences were determined using one-way ANOVA followed by Tukey's multiple comparisons test.

three weeks, followed by two weeks of normal chow. A Laquinimod solution was administered daily by oral gavage (200 µl; 25 mg/kg) during week 1–3. (D) CupEAE/Vehicle, animals were intoxicated with cuprizone and treated with vehicle solution as described for group B. At the beginning of week six, the mice were immunized with $MOG_{35–55}$ peptide as published previously (Ruther et al., 2017; Scheld et al., 2016). (E) CupEAE/Laquinimod, animals were intoxicated with cuprizone and treated with Laquinimod solution as described for group C. At the beginning of week six, the mice were immunized with $MOG_{35–55}$ peptide. Laquinimod was provided from Teva Pharmaceutical Industries, LTd., Petah Tikva, Israel and was dissolved at 2.5 mg/ml in purified water. The dosing regimen was selected based on a previous report (Wegner et al., 2010).

2.2. Cuprizone intoxication and EAE induction

To induce neurodegeneration of the forebrain, mice were intoxicated with the copper chelator Cuprizone (bis(cyclohexanone)oxaldihydrazone; Sigma-Aldrich, Taufkirchen, Germany) as previously published by our group (Hochstrasser et al., 2017; Slowik et al., 2015). In brief, 0.25 g cuprizone was weighed using precision scales and mechanically mixed with 100 g ground standard rodent chow using a commercial available kitchen machine (Kult X, WMF Group, Geislingen an der Steige, Germany). The chow was mixed at low speed and manual agitation for 1 min and was provided within the cage in two separate plastic Petri dishes.

The formation of myelin autoreactive T cells was achieved by immunization with an emulsion of Myelin oligodendrocyte glycoprotein (MOG) peptide dissolved in complete Freund's adjuvant (CFA), followed by intraperitoneal injection of pertussis toxin (PTX) in phosphate-buffered saline (PBS), first on the day of immunization and then again the following day (i.e., active EAE). A ready-to-use kit provided by Hooke Laboratories was used. Scoring of disease severity was performed daily as published previously (Barthelmes et al., 2016; Beeton et al., 2007) as follows: A score of 0.5 was assigned if the tip of the tail was limb when the mouse was picked up by the base of the tail; a score of 1 was assigned if the entire tail dropped over the finger of the observer when the mouse was picked up by the base of the tail; when the mouse was dropped on a wire rack, and at least one hind leg fell through consistently, a score of 1.5 was given; a score of 2 was assigned when the legs of the mice were not spread apart but held close together when the mouse was picked up by the base of the tail, or when the mice exhibited a clearly apparent wobbly gait; a score of 2.5 was assigned when the tail was limp and both hind legs had movement, but were dragging at the feet, or one hind leg showed complete paralysis, whereas the other one still showed movement; a score of 3 was assigned when the tail was limp and the mice showed complete paralysis of hind legs; a score of 3.5 was given if the mouse was unable to raise itself when placed on its side; a score of 4 was assigned if the tail was limp and the mice showed complete hind leg and partial front leg paralysis, and the mouse was minimally moving around the cage but appeared alert; a score of 4.5 was given if the mouse showed no movement around the cage and appeared not alert.

2.3. Tissue preparation

Mice were deeply anaesthetized with ketamine (100 mg/kg i.p.) and xylazine (10 mg/kg i.p.) and transcardially perfused with ice-cold PBS followed by a 3.7% paraformaldehyde solution (PFA; pH 7.4). The brains and spinal cords were postfixed in the same fixative at 4 °C, carefully dissected and embedded in paraffin. Then, sections of 5 µm were prepared for histological investigations. Brains were sectioned at the levels 215 up to 265 according to the mouse brain atlas by Sidman et al. (http://www.hms.harvard.edu/research/brain/atlas.html). Region 215 corresponds to the stereotaxic coordinates Bregma +0.14, whereas region 265 corresponds to the stereotaxic coordinates Bregma −1.01, provided by Franklin and Paxinos.

2.4. Histology and immunohistochemistry

For histological evaluations, randomly selected brain sections containing the region of interest (ROI) were stained with standard Luxol fast blue-periodic acid-Schiff (LFB/PAS) to determine demyelination, and hematoxylin & eosin (H&E) to quantify the number and spatial distribution of perivascular infiltrates within the forebrain. Spinal cord sections were stained with LFB/PAS to evaluate inflammatory demyelination within the white matter.

Immunohistochemistry was performed using the following antibodies: Anti-Ionized calcium-binding adaptor molecule 1 (IBA1) and anti-MAC3 to visualize microglia and macrophages, anti-Vimentin, anti-glial fibrillary acidic protein (GFAP) and anti-Aldehyde Dehydrogenase 1 Family Member L1 (ALDH1L1) to study the signature of astrocyte activation, anti-CD4 to visualize T-helper cells, and anti-amyloid precursor protein (APP), anti-vesicular glutamate transporter 1 (vGLUT1) and anti-Synaptophysin to detect acutely damaged axons. The stains were conducted following established protocols (Nyamoya et al., 2019; Ruther et al., 2017). In brief, the sections were rehydrated, and if necessary, antigens were unmasked by heating in either Tris/EDTA (pH 9.0) or citrate (pH 6.0) buffer. After washing in PBS, unspecific binding sites were blocked in blocking solution (serum of the species in which the secondary antibody was produced) for 1 h. Then, the sections were incubated overnight (at 4 °C) with the primary antibodies diluted in blocking solution. The next day, the slides were treated with 0.3% hydrogen peroxide in PBS for 30 min. After washing in PBS, the slides were incubated with biotinylated secondary antibodies for 1 h and then with peroxidase-coupled avidin-biotin complex (ABC kit; Vector Laboratories, Peterborough, UK). Anti-vGLUT1 and anti-Synaptophysin stains were performed using HRP-linked goat anti-mouse IgG secondary antibodies (Dako, Germany). The primary and secondary antibodies used in this study are listed in Tables 1 and 2. Finally, the sections were treated with 3,3′-diaminobenzidine (DAKO, Hamburg, Germany) as a peroxidase substrate. Appropriate negative controls (without primary antibodies or with isotype antibodies) were performed in parallel as previously described (Baertling et al., 2010) to ensure specificity of the staining.

2.5. Histological evaluations

All analyses were performed with coronal sections at the levels R215 and R265 using a Nikon ECLIPSE 50i microscope (Nikon Instruments, Düsseldorf, Germany) equipped with a DS-2Mv camera. The following ROIs were defined: midline of the corpus callosum (CC), lateral corpus callosum, subcortex, and primary somato-sensory cortex. To estimate demyelination in LFB/PAS stains, a nonparametric grading

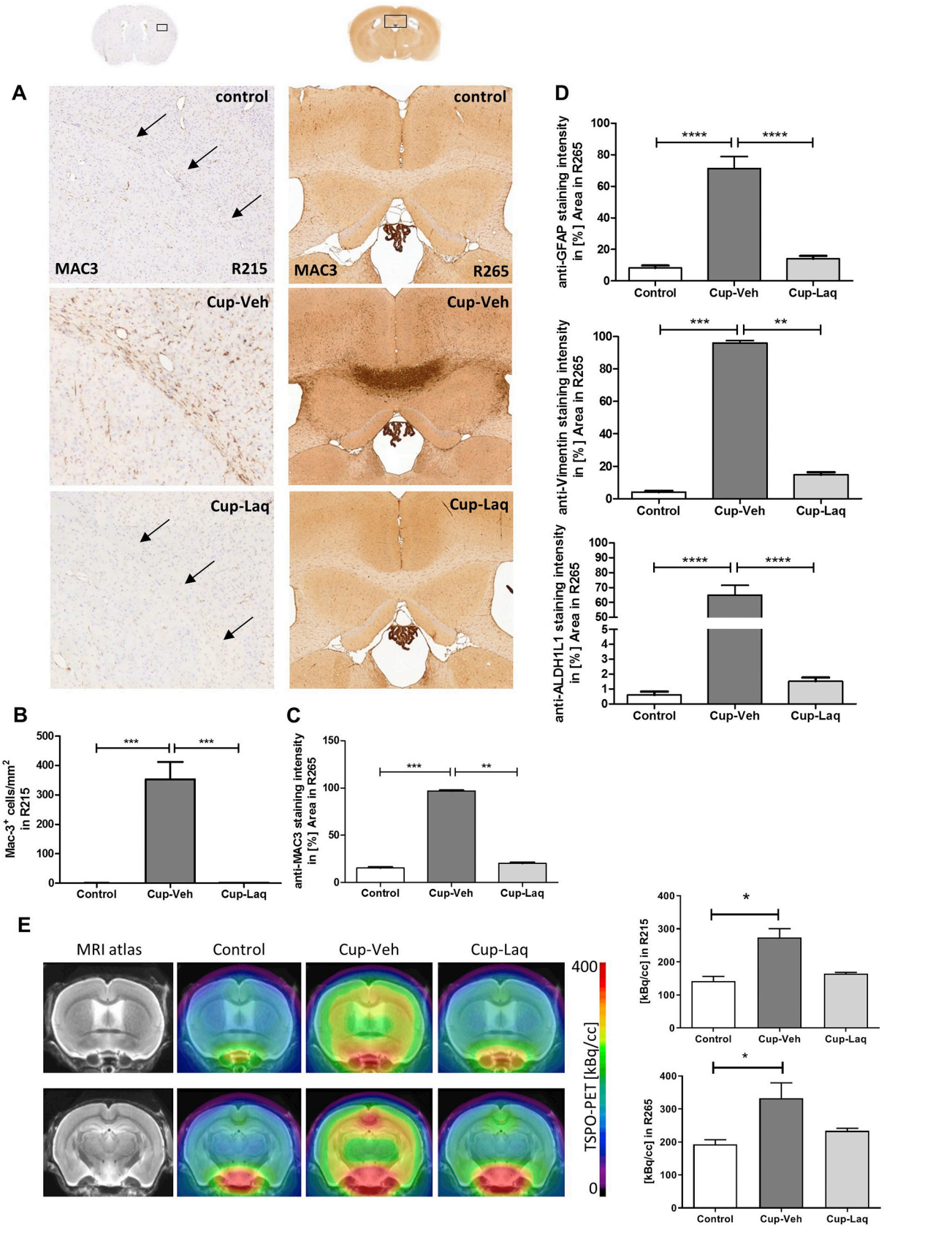

(caption on next page)

Fig. 2. Laquinimod ameliorates cuprizone-induced gliosis.
(A) Representative anti-MAC3 stains of the lateral CC (region 215; left) and midline of the CC (region 265; right). Arrows highlight the lateral part of the CC in region 215. (B/C) Extent of microglia activation, determined in anti-MAC3 stained sections (R215 in B and R265 in C; control: $n = 5/4$, Cup-Veh: $n = 9/11$, Cup-Laq: n = 10/10). Differences were determined using Kruskal-Wallis-Test followed by Dunn's multiple comparisons test. (D) Extent of astrocyte activation, determined in anti-GFAP (upper graph), anti-Vimentin (middle graph) or anti-ALDH1L1 (lower graph) processed sections (control: n = 5, Cup-Veh: $n = 11$, Cup-Laq: n = 10). Differences for anti-GFAP and anti-ALDH1L1 stains were determined using one-way ANOVA followed by Tukey's multiple comparisons test. Differences for anti-Vimentin stains were determined using Kruskal-Wallis-Test followed by Dunn's multiple comparisons test. (E) Quantification of [^{18}F]-GE-180 radioligand uptake in control, Cup-Veh and Cup-Laq mice ($n = 4$ animals per group). Averaged normalized radioligand uptake per group is shown for the lateral CC (region 215; upper row) and for the midline of the CC (region 265; lower row). Coronal slices are depicted upon an MRI atlas. Differences for [^{18}F]-GE-180 radioligand uptake values were determined using Kruskal-Wallis-Test followed by Dunn's multiple comparisons test. Please note that activity spilling into the hypothalamus is related to unspecific uptake in the hypophysis. The unspecific binding has to be considered when regions adjacent to the hypophysis are considered for evaluation but it had no impact on the current analysis.

approach was performed by two independent and blinded evaluators. In region 215, the lateral CC was defined as ROI and the slides were scored on a scale from 1 (normal myelination) to 5 (most severe demyelination; see supplementary Fig. 2A). In region 265, the midline of the CC was defined as the ROI and the slides were sorted by one blinded evaluator in ascending order of the extent of demyelination. In H&*E*-stains, the number of perivascular infiltrates within the forebrain was quantified between the levels 215 and 265 by two blinded observers and the results were averaged. To analyze cell/spheroid densities in immunohistochemically processed sections, the ROI-area was manually outlined using ImageJ (NIH, Bethesda, MD, USA), and positive cells were counted by at least two evaluators blinded to the treatment groups. The results were averaged and are shown as cells/mm^2. Since defining individual cells in the fully demyelinated corpus callosum was sometimes challenging (mainly at the level R265), in some cases staining intensities were quantified by densitometrical analyses. Therefore, binary-converted pictures were evaluated within the ROI using ImageJ. A value of 100% represents a maximum and 0% a minimum of staining intensity. Results are shown as staining intensity in [%] Area of the entire ROI.

Spinal cord sections were stained with LFB/PAS to visualize intact and damaged myelin plus inflammatory infiltrates. The extent of inflammatory demyelination was quantified by measuring an inflammatory-demyelination index, which is defined as the area covered by inflammatory demyelination in relation to the entire white matter area of each slide (see supplementary Fig. 2B). The index was measured in two slides per animal by two different observers, and then averaged.

2.6. Positron emission tomography (PET)—imaging

Four mice per group of controls, Cup/Veh and Cup/Laquinimod underwent PET after week 5 of the experimental setup. All rodent PET procedures followed an established standardized protocol for radiochemistry, acquisition and post-processing (Brendel et al., 2016; Overhoff et al., 2016). In brief, [^{18}F]-GE-180 TSPO-PET (11.8 ± 2.2 MBq) with an emission window of 60–90 min p.i. was used to measure cerebral glial activity by a Siemens Inveon DPET (Siemens, Knoxville, Tennessee). All analyses were performed using PMOD (V3.5, PMOD technologies, Basel, Switzerland). Normalization of the injected activity was performed by the previously validated myocardium correction method (Deussing et al., 2018). TSPO-PET values, deriving from predefined volumes of interest (VOI; medial corpus callosum = 7.7 mm^3, analogous to the R265 ROI and bihemispheric lateral corpus callosum = 3.7 mm^3 each, analogous to the R215 ROI) were extracted and compared between the groups.

2.7. Statistical analyses

All data are given as arithmetic means ± SEMs. Differences between groups were statistically tested using Prism 5 (GraphPad Software Inc., San Diego, CA, USA). *p*-values of < 0.05 were considered to be statistically significant. The following symbols are used to indicate the level of significance: $*p < .05$, $**p < 0.01$, $***p < 0.001$, ns indicates 'not significant'. No outliers were excluded from the analyses. The Shapiro-Wilk test was applied to test for normal data distribution. Applied statistical tests are given in the respective figure legends.

3. Results

It has previously been shown that Laquinimod ameliorates anti $MOG_{35–55}$ immune responses in EAE mice (Kaye et al., 2016). First, we were interested whether Laquinimod is as well protective in a model of metabolic oligodendrocyte injury. To this end, mice were intoxicated with cuprizone for three weeks, and thereafter put on normal chow for another two weeks. During the three weeks cuprizone intoxication period, one group was treated with vehicle solution (group B in supplementary Fig. 1), and another group was treated daily with Laquinimod (25 mg/kg; group C). After week 5, the mice were sacrificed and their brains were analyzed for demyelination and the activation of microglia cells at two distinct brain levels (i.e., R215 and R265).

At the levels of the anterior commissure (i.e., R215) a severe loss of LFB-staining intensity, suggestive for demyelination, was observed in the lateral parts of the corpus callosum (see Fig. 1A, left column and Fig. 1B), whereas at the level of the rostral hippocampus (i.e., R265; see Fig. 1A, right column and Fig. 1C) LFB-staining intensity loss was severe within medial parts of the corpus callosum. Demyelination was paralleled by the accumulation of IBA1$^+$ microglia which was particularly pronounced at the level of the rostral hippocampus (Fig. 1D–F). Both cuprizone-induced pathologies were significantly ameliorated by the Laquinimod-treatment. To verify reduced microglia activities in Laquinimod-treated mice, serial sections were processed for anti-MAC3 immunohistochemistry, which labels activated microglia cells and monocytes. As demonstrated in Fig. 2A–C, at both brain levels pronounced anti-MAC3 staining intensity was observed in vehicle- but not Laquinimod-treated cuprizone mice. Furthermore, Laquinimod prevented cuprizone-induced astrocyte activation, as demonstrated by anti-GFAP, anti-Vimentin and anti-ALDH1L1 immunohistochemistry (see Fig. 2D), respectively. To further substantiate the finding of a protective Laquinimod effect in the cuprizone model, activated microglia and astrocytes were additionally visualized by [^{18}F]-GE-180-PET imaging as described recently by our group (Nack et al., 2019). As demonstrated in Fig. 2E, we found a significant increase of [^{18}F]-GE180 uptake in the medial and lateral corpus callosum of Cup/Veh but not Cup/Laq mice. In summary, these results clearly show that Laquinimod almost completely ameliorates the cuprizone-induced myelin pathology.

To understand, whether the observed protective effect of Laquinimod in the cuprizone model results in less severe peripheral immune cell recruitment if encephalitogenic T cells are induced in the peripheral lymphoid organs, in a next step we repeated the experiments as described above but immunized both cohorts at the beginning of week 6 with $MOG_{35–55}$ peptide dissolved in CFA + PTX (i.e., active EAE induction; groups D and E in supplementary Fig. 1). Of note, peripheral immune cells do not invade the forebrain in classical $MOG_{35–55}$-induced EAE (Ruther et al., 2017; Scheld et al., 2016). First, we verified that active $MOG_{35–55}$ induces a comparable active immune response in

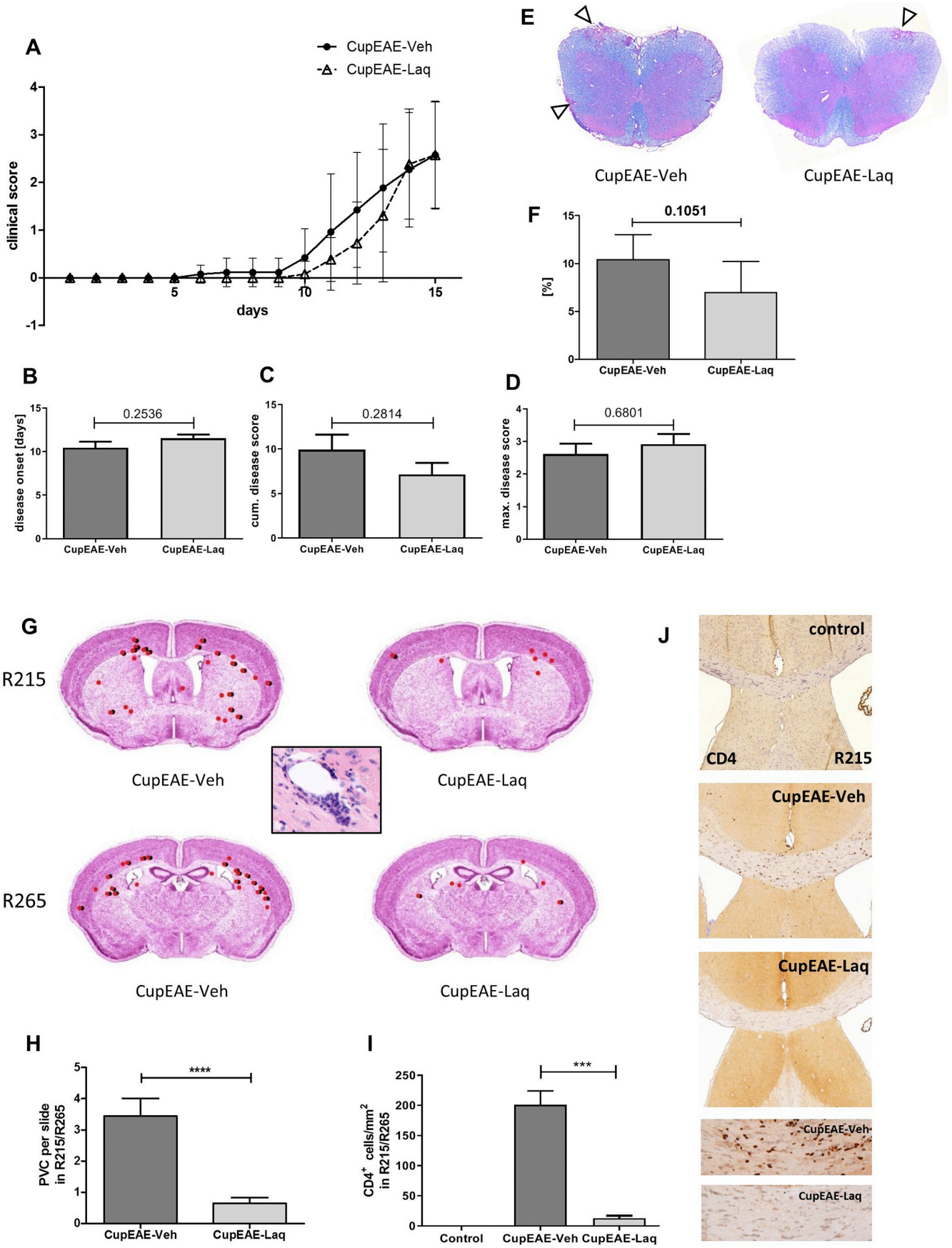

(caption on next page)

Fig. 3. Laquinimod ameliorates secondary immune cell recruitment.
(A) Clinical scores for CupEAE-Veh (black circle) and CupEAE-Laq (white triangle) mice. Quantification of the parameters *day of disease onset* (B), *cumulative disease scores* (C) and *maximum disease score*. $N = 13$ per experimental group. Differences were determined using Mann Whitney test. (E) Representative LFB/PAS stains of the spinal cord. Arrowheads mark inflammatory infiltrates. (F) Extent of inflammatory demyelination in CupEAE-Veh (n = 10) and CupEAE-Laq (n = 10) mice. Differences were determined using Mann Whitney test. (G) Spatial distribution of perivascular infiltrates in the different treatment groups (H&E staining; black and red dots from one independent observer each) at two brain levels (regions according to Sidman et al.). $N = 5$ animals per experimental group. A representative perivascular infiltrate is demonstrated in the center of the image. (H) Numbers of perivascular infiltrates in CupEAE-Veh and CupEAE-Laq groups. N = 13 per experimental group. Differences were determined using Mann Whitney test. (I) Numbers of $CD4^+$ lymphocytes in CupEAE-Veh and CupEAE-Laq groups. N = 13 per experimental group. Differences were determined using Mann Whitney test. (J) Representative anti-CD4 stained images to demonstrate T_h-cell recruitment in CupEAE-Veh and CupEAE-Laq mice. Lower parts of the image show the midline of the corpus callosum in higher magnification.

vehicle and Laquinimod-treated mice. As shown in Fig. 3A–D, the severity of clinical symptoms was comparable in both genotypes. In particular, no significant difference was observed for the parameters day of disease onset (CupEAE-Veh 10.5 ± 2.5 vs. CupEAE-Laq 11.5 ± 1.6; $p = 0.25$), cumulative disease score (CupEAE-Veh 10.0 ± 6.0 vs. CupEAE-Laq 7.2 ± 4.7; $p = 0.28$) and maximum disease score (CupEAE-Veh 2.6 ± 1.2 vs. CupEAE-Laq 2.9 ± 1.1; $p = 0.68$). In line with this finding, there was no significant difference in the extent of inflammatory infiltrates in the spinal cord of CupEAE-Veh vs. CupEAE-Laq mice (Fig. 3E–F). Next, we analyzed the forebrain at distinct rostral-to-caudal levels for the presence of perivascular infiltrates, a hallmark of active MS lesions. In line with previous observations, several perivascular infiltrates were present in the forebrains of CupEAE-Veh animals. Such infiltrates were topographically distributed widely, including the cortex, CC and subcortical regions (Fig. 3G). Remarkably, the number of perivascular infiltrates was significantly lower in CupEAE-Laq compared to CupEAE-Veh animals (Fig. 3H). Whereas in CupEAE-Veh animals the average number of perivascular cuffs per slide was 3.4 ± 2.9, CupEAE-Laq animals contained 0.7 ± 0.9 perivascular cuffs per slide ($p \leq 0.0001$). To substantiate our finding of less severe peripheral immune cell recruitment in the CupEAE-Laq group, brain sections were processed for anti-CD4 immunohistochemistry to label T_h-lymphocytes. Densities of $CD4^+$ lymphocytes were significantly increased in CupEAE-Veh but not CupEAE-Laq mice. Lower $CD4^+$ cell densities in Laquinimod-treated mice were found at various topographical sites including the corpus callosum (Fig. 3I/J), cortex and subcortex (data not shown).

Finally, we were interested whether neurodegeneration is ameliorated in Laquinimod-treated CupEAE mice. The extent of acute axonal injury was analyzed by quantifying the densities of axonal swellings in anti-APP stained sections. As demonstrated in Fig. 4A–C, APP^+ spheroids were virtually absent in control animals, whereas numerous were found in CupEAE/Veh mice. Of note, just some APP^+ spheroids were observed in CupEAE-Laq mice. To substantiate this observation, we additionally stained sections of CupEAE-Veh and CupEAE-Laq mice against the vesicular glutamate transporter 1 (vGLUT1) and Synaptophysin, also known as the major synaptic vesicle protein p38. As recently shown, both synaptic proteins accumulate as spheroids within acutely injured axons (Gudi et al., 2017; Ruhling et al., 2019). As demonstrated in Fig. 4D–G, high densities of $vGLUT1^+$ and $Synaptophysin^+$ spheroids were found in CupEAE-Veh but not CupEAE-Laq mice. These data clearly demonstrate a neuroprotective effect of Laquinimod in the applied model.

4. Discussion

In this study, we demonstrated that oral Laquinimod treatment ameliorates inflammatory demyelination and neurodegeneration in a novel MS animal model which is characterized by multi-focal perivascular inflammation in the entire CNS, most importantly in the forebrain (Chrzanowski et al., 2019; Ruther et al., 2017; Scheld et al., 2016). Furthermore, we verified previous findings demonstrating that Laquinimod prevents cuprizone-induced demyelination (Bruck et al., 2012; Kramann et al., 2016).

Our group and others recently demonstrated that primary oligodendrocyte degeneration can trigger peripheral immune cell recruitment into the forebrain in $MOG_{35–55}$ immunized mice (Baxi et al., 2015; Boretius et al., 2012; Ruther et al., 2017; Scheld et al., 2016). In these studies, oligodendrocyte apoptosis in the brains of mice was first induced by a 3-week intoxication with cuprizone, and an infiltration of myelin autoreactive T cells from peripheral lymphoid organs was then triggered via immunization with the $MOG_{35–55}$ peptide. In the current study we were now interested to see whether amelioration of the cuprizone-induced pathology by Laquinimod results in less severe secondary peripheral immune cell recruitment.

Our observation of a strong protective Laquinimod effect in the cuprizone model is in line with previous observations. Brück and colleagues nicely demonstrated that Laquinimod prevents cuprizone-induced demyelination, microglial activation and axonal degeneration (Bruck et al., 2012; Kramann et al., 2016). Further mechanistic studies suggested that the protective effect of Laquinimod in the cuprizone model is mediated by a modulation of astrocyte function, in particular by attenuating astrocytic NF-κB activation. We verify the observation of a protective Laquinimod effect in the cuprizone model but additionally show that the pharmacological amelioration of the cuprizone-induced pathology secondary results in less severe peripheral immune cell recruitment. This important and novel finding suggests that therapeutic strategies, which ameliorate brain intrinsic inflammatory responses (i.e., astrocyte and/or microglia activation), at the same time can decrease the recruitment of peripheral immune cells, in particular lymphocytes. Histopathological studies revealed that during progressive MS, T and B cells can still be found within the CNS parenchyma, and that the densities of T- and B-cells positively correlate with the level of acute axonal injury (Frischer et al., 2009). Understanding the relation between inflammation and neurodegeneration is of key importance for future therapeutic strategies in MS. If inflammation drives subsequent neurodegeneration, proper anti-inflammatory therapies are the best choice to stop the disease and to prevent further clinical deterioration of the patients. Results of this study, however, suggest that the opposite might equally be true: Amelioration of brain-intrinsic degenerative cascades might secondary reduce the level of inflammation in the CNS.

We additionally show that the protective effects of Laquinimod can be visualized in vivo via PET-imaging using the TSPO tracer [^{18}F]-GE-180. As demonstrated in Fig. 2, [^{18}F]-GE-180 radioligand uptake was significantly increased in cuprizone + vehicle but not in cuprizone + Laquinimod groups, compared to controls. The cellular source of TSPO expression, and hence TSPO-ligand binding in the CNS of MS patients is not entirely clear. While most studies suggest that TSPO is predominantly expressed by activated microglia cells and in consequence an increase in TSPO ligand binding is interpreted as microglia activation (Abourbeh et al., 2012; Airas et al., 2015; Blume et al., 2018; Klein et al., 2018; Mattner et al., 2013), various other cell types have been shown to express TSPO as well, among astrocytes (Mattner et al., 2011; Notter et al., 2018). In recent works, we and others were able to demonstrate that in the cuprizone model an increase in TSPO expression is found in different cell types including microglia and astrocytes (Nack et al., 2019; Zinnhardt et al., 2019). In line with this, on the immunohistological level, we found reduced microglia and astrocyte reactivity in Laquinimod compared to vehicle-treated mice which likely contributes to the decreased tracer signal.

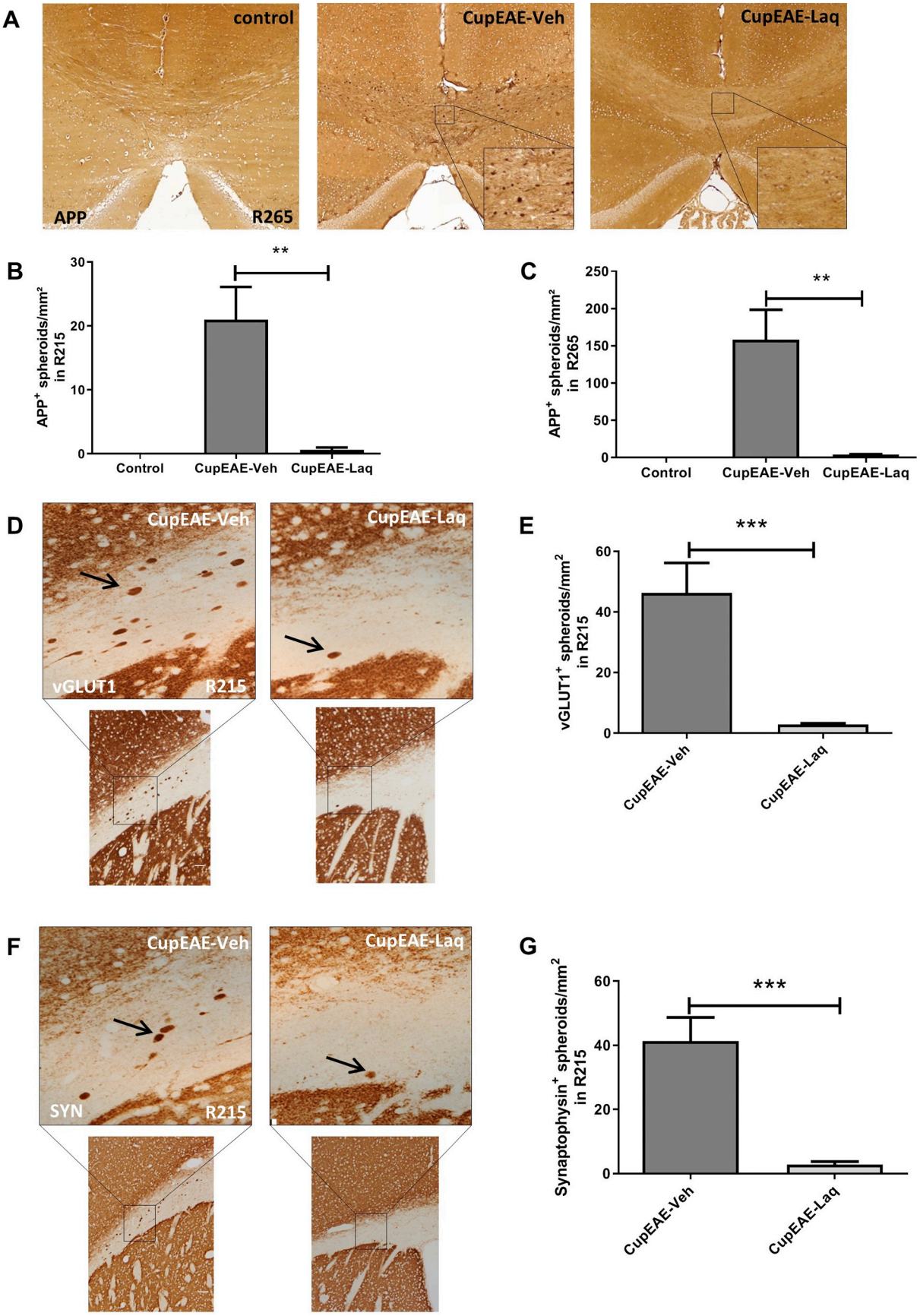

(caption on next page)

Fig. 4. Laquinimod ameliorates axonal damage.
(A) Representative anti-APP stains of the medial CC (region 265). The high-power insets show representative parts of the medial CC in higher magnification. (B/C) Extent of axonal damage, determined in anti-APP stained sections (R215 in B and R265 in C; control: n = 5/5, Cup-Veh: n = 4/5, Cup-Laq: n = 5/5). (D) Representative anti-vGLUT1 stains of the lateral CC (region 215). The high-power insets show representative parts of the lateral CC in higher magnification. (E) Extent of axonal damage, determined in anti-vGLUT1 stained sections (R215; CupEAE-Veh: *n* = 8, CupEAE-Laq: n = 8). (F) Representative anti-Synaptophysin stains of the lateral CC (region 215). The high-power insets show representative parts of the lateral CC in higher magnification. (E) Extent of axonal damage, determined in anti-Synaptophysin stained sections (R215; CupEAE-Veh: n = 8, CupEAE-Laq: n = 8). Differences were determined using Mann Whitney test.

Quinoline-3-carboxamide derivatives such as Laquinimod, Tasquinimod or Paquinimod have shown immunomodulatory effects in different pre-clinical animal models (Helmersson et al., 2013; Ott et al., 2019). In a recent study it was shown that Laquinimod ameliorates EAE by activating the aryl hydrocarbon receptor (Kaye et al., 2016). In the same study the authors demonstrated by using bone marrow chimeras that deletion of the aryl hydrocarbon receptor in the immune system fully abrogates, whereas deletion within the CNS partially abrogates the protective effect of Laquinimod in EAE. These results suggest that Laquinimod has both, immunosuppressive and neuroprotective properties. In line with a proposed central protective effect, Laquinimod has been shown to be protective in models of Huntington Disease (Garcia-Miralles et al., 2017; Garcia-Miralles et al., 2019). As outlined in the introduction section of this manuscript, two independent clinical studies demonstrated that Laquinimod is effective in suppressing development of active lesions in relapsing-remitting MS (Comi et al., 2008; Polman et al., 2005). Of note, the two phase 3 studies BRAVO and ALLEGRO showed modest effects of Laquinimod on measures of focal inflammatory disease activity, but more robust effects on reducing brain atrophy and, possibly, disability worsening (Comi et al., 2012; Vollmer et al., 2014). It is well known that the recruitment of peripheral immune cells can lead to degeneration of neurons. For example, Siffrin and colleagues nicely demonstrated that in EAE, the direct interaction of MOG-specific Th17 and neuronal cells in demyelinating lesions is associated with extensive axonal damage (Siffrin et al., 2010). Our results, however, show that an opposite scenario might as well be possible, that is: neurodegeneration can trigger the formation of new, focal inflammatory lesions. Importantly, the clinical efficacy profile of Laquinimod derived from the two relapsing-remitting MS studies, ALLEGRO and BRAVO, is distinctive and different from other disease modifying treatments in MS because the reduction in disease progression is consistently larger than expected based on the relapse based outcomes. We, thus, speculate that the neuroprotective effect of Laquinimod (i.e., reduction in brain atrophy) in the BRAVO and ALLEGRO phase 3 studies did, secondary, lead to the observed reduced inflammatory activity.

We would like to emphasize at that point that the reduced inflammatory activity in the forebrain of Laquinimod-treated Cup/EAE mice is most likely not due to an immunosuppressive effect of Laquinimod. As shown in Fig. 3, both surrogate markers for $MOG_{35–55}$ induced autoimmunity, clinical EAE score and extent of inflammatory demyelination in the spinal cord, was not significantly modulated by Laquinimod treatment. This might, on the first view, be contradicting to the previously reported immunosuppressive effects of Laquinimod in EAE (Thone et al., 2012; Yang et al., 2004; Zou et al., 2002). However, in the current study Laquinimod treatment was terminated two weeks prior to active EAE induction (see supplementary Fig. 1). We, thus, assume that two weeks were enough to reduce Laquinimod levels in the body to an extent where it is not immunosuppressive any more. Indeed, results of clinical studies suggest that high doses of Laquinimod are required to exert its full anti-inflammatory activity (Comi et al., 2008). Furthermore, pharmacokinetic studies in mice showed a relatively short half-time of Laquinimod (Brunmark et al., 2002). In particular, oral administration of 5 mg/kg to female SJL/N mice led to a peak plasma concentration of 25 μM. As soon as 15 h post application, Laquinimod's plasma concentration was lower than 2 μM. As demonstrated in Fig. 2, the cumulative disease score tended to be lower in Laquinimod-treated compared to vehicle-treated CupEAE mice. However, statistical comparison of both groups revealed no significant difference (p = 0.2814). It might principally be that too few mice were included to determine whether Laquinimod indeed suppresses anti-$MOG_{35–55}$ immune responses. In other words, our study could lack sufficient statistical power to detect a potential Laquinimod effect on the cumulative disease score. Thus, we cannot rule out a minor immunosuppressive effect of Laquinimod in Cup/EAE mice, but such a minor effect, if present, would not explain the pronounced protective effect of Laquinimod on the level of the forebrain in Cup/EAE mice.

In summary, this study clearly illustrates that amelioration of a primary brain-intrinsic degenerative process secondary halts peripheral immune cell recruitment and, in consequence, inflammatory lesion development. These findings have important consequences for the interpretation of the results of clinical studies.

Supplementary data to this article can be found online at https://doi.org/10.1016/j.nbd.2019.104675.

Acknowledgments

The technical support from A. Baltruschat, B. Aschauer and S. Wübbel is acknowledged. GE made GE-180 cassettes available through an early access model. This study was supported by the Dr. Robert Pfleger Stiftung (M.K.) and the Deutsche Forschungsgemeinschaft (KI 1469/8-1).

References

Aboul-Enein, F., et al., 2003. Preferential loss of myelin-associated glycoprotein reflects hypoxia-like white matter damage in stroke and inflammatory brain diseases. J. Neuropathol. Exp. Neurol. 62, 25–33.
Abourbeh, G., et al., 2012. Imaging microglial/macrophage activation in spinal cords of experimental autoimmune encephalomyelitis rats by positron emission tomography using the mitochondrial 18 kDa translocator protein radioligand [(1)(8)F]DPA-714. J. Neurosci. 32, 5728–5736.
Airas, L., et al., 2015. In vivo PET imaging demonstrates diminished microglial activation after fingolimod treatment in an animal model of multiple sclerosis. J. Nucl. Med. 56, 305–310.
Baertling, F., et al., 2010. ADAM12 is expressed by astrocytes during experimental demyelination. Brain Res. 1326, 1–14.
Barthelmes, J., et al., 2016. Induction of experimental autoimmune encephalomyelitis in mice and evaluation of the disease-dependent distribution of immune cells in various tissues. J. Vis. Exp. 111. https://doi.org/10.3791/53933.
Baxi, E.G., et al., 2015. Transfer of myelin-reactive th17 cells impairs endogenous remyelination in the central nervous system of cuprizone-fed mice. J. Neurosci. 35, 8626–8639.
Beeton, C., et al., 2007. Induction and clinical scoring of chronic-relapsing experimental autoimmune encephalomyelitis. J. Vis. Exp. 224.
Blume, T., et al., 2018. Microglial response to increasing amyloid load saturates with aging: a longitudinal dual tracer in vivo muPET-study. J. Neuroinflammation 15, 307.
Boretius, S., et al., 2012. Assessment of lesion pathology in a new animal model of MS by multiparametric MRI and DTI. Neuroimage. 59, 2678–2688.
Brendel, M., et al., 2016. Glial activation and glucose metabolism in a transgenic amyloid mouse model: a triple-tracer PET study. J. Nucl. Med. 57, 954–960.
Bruck, W., et al., 2012. Reduced astrocytic NF-kappaB activation by laquinimod protects from cuprizone-induced demyelination. Acta Neuropathol. 124, 411–424.
Brunmark, C., et al., 2002. The new orally active immunoregulator laquinimod (ABR-215062) effectively inhibits development and relapses of experimental autoimmune encephalomyelitis. J. Neuroimmunol. 130, 163–172.
Chrzanowski, U., et al., 2019. Oligodendrocyte degeneration and concomitant microglia activation directs peripheral immune cells into the forebrain. Neurochem. Int. 126, 139–153. https://doi.org/10.1016/j.neuint.2019.03.005. Epub 2019 Mar 10.
Comi, G., et al., 2008. Effect of laquinimod on MRI-monitored disease activity in patients with relapsing-remitting multiple sclerosis: a multicentre, randomised, double-blind, placebo-controlled phase IIb study. Lancet. 371, 2085–2092.
Comi, G., et al., 2012. Placebo-controlled trial of oral laquinimod for multiple sclerosis. N.

Engl. J. Med. 366, 1000–1009.
Deussing, M., et al., 2018. Coupling between physiological TSPO expression in brain and myocardium allows stabilization of late-phase cerebral [(18)F]GE180 PET quantification. Neuroimage. 165, 83–91.
Di Filippo, M., et al., 2018. Multiple sclerosis and cognition: synaptic failure and network dysfunction. Nat. Rev. Neurosci. 19, 599–609.
Ellrichmann, G., et al., 2017. Laquinimod treatment in the R6/2 mouse model. Sci. Rep. 7, 4947.
Filippi, M., et al., 2014. Placebo-controlled trial of oral laquinimod in multiple sclerosis: MRI evidence of an effect on brain tissue damage. J. Neurol. Neurosurg. Psychiatry 85, 851–858.
Frischer, J.M., et al., 2009. The relation between inflammation and neurodegeneration in multiple sclerosis brains. Brain. 132, 1175–1189.
Fu, L., et al., 1998. Imaging axonal damage of normal-appearing white matter in multiple sclerosis. Brain. 121 (Pt 1), 103–113.
Garcia-Miralles, M., et al., 2017. Early pridopidine treatment improves behavioral and transcriptional deficits in YAC128 Huntington disease mice. JCI Insight. 2.
Garcia-Miralles, M., et al., 2019. Laquinimod treatment improves myelination deficits at the transcriptional and ultrastructural levels in the YAC128 mouse model of Huntington disease. Mol. Neurobiol. 56 (6), 4464–4478. https://doi.org/10.1007/s12035-018-1393-1. Epub 2018 Oct 17.
Gudi, V., et al., 2017. Synaptophysin is a reliable marker for axonal damage. J. Neuropathol. Exp. Neurol. https://doi.org/10.1093/jnen/nlw114. Epub ahead of print.
Helmersson, S., et al., 2013. Amelioration of experimental autoimmune encephalomyelitis by the quinoline-3-carboxamide paquinimod: reduced priming of proinflammatory effector CD4(+) T cells. Am. J. Pathol. 182, 1671–1680.
Katsumoto, A., et al., 2018. Laquinimod attenuates inflammation by modulating macrophage functions in traumatic brain injury mouse model. J. Neuroinflammation 15, 26.
Kaye, J., et al., 2016. Laquinimod arrests experimental autoimmune encephalomyelitis by activating the aryl hydrocarbon receptor. Proc. Natl. Acad. Sci. U. S. A. 113, E6145–e6152.
Kipp, M., et al., 2012. Pathology of multiple sclerosis. CNS Neurol. Disord Drug Targets. 11, 506–517.
Klein, B., et al., 2018. Age influences microglial activation after Cuprizone-induced demyelination. Front. Aging Neurosci. 10, 278.
Kramann, N., et al., 2016. Laquinimod prevents cuprizone-induced demyelination independent of Toll-like receptor signaling. Neurol. Neuroimmunol. Neuroinflamm. 3, e233.
Mattner, F., et al., 2011. Evaluation of [(1)(2)(3)I]-CLINDE as a potent SPECT radiotracer to assess the degree of astroglia activation in cuprizone-induced neuroinflammation. Eur. J. Nucl. Med. Mol. Imaging 38, 1516–1528.
Mattner, F., et al., 2013. Central nervous system expression and PET imaging of the translocator protein in relapsing-remitting experimental autoimmune encephalomyelitis. J. Nucl. Med. 54, 291–298.
Moore, S., et al., 2013. Therapeutic laquinimod treatment decreases inflammation, initiates axon remyelination, and improves motor deficit in a mouse model of multiple sclerosis. Brain Behav. 3, 664–682.
Nack, A., et al., 2019. Expression of translocator protein and [18F]-GE180 ligand uptake in multiple sclerosis animal models. Cells. 8.
Notter, T., et al., 2018. Translational evaluation of translocator protein as a marker of neuroinflammation in schizophrenia. Mol. Psychiatry 23, 323–334.
Nyamoya, S., et al., 2019. G-protein-coupled receptor Gpr17 expression in two multiple sclerosis remyelination models. Mol. Neurobiol. 56, 1109–1123.
Ott, M., et al., 2019. Laquinimod, a prototypic quinoline-3-carboxamide and aryl hydrocarbon receptor agonist, utilizes a CD155-mediated natural killer/dendritic cell interaction to suppress CNS autoimmunity. J. Neuroinflammation 16, 49.
Overhoff, F., et al., 2016. Automated spatial brain normalization and hindbrain white matter reference tissue give improved [(18)F]-Florbetaben PET quantitation in Alzheimer's model mice. Front. Neurosci. 10, 45.
Polman, C., et al., 2005. Treatment with laquinimod reduces development of active MRI lesions in relapsing MS. Neurology. 64, 987–991.
Ruffini, F., et al., 2013. Laquinimod prevents inflammation-induced synaptic alterations occurring in experimental autoimmune encephalomyelitis. Mult. Scler. 19, 1084–1094.
Ruhling, S., et al., 2019. Visualization of the breakdown of the axonal transport machinery: a comparative ultrastructural and immunohistochemical approach. Mol. Neurobiol. 56, 3984–3998.
Ruther, B.J., et al., 2017. Combination of cuprizone and experimental autoimmune encephalomyelitis to study inflammatory brain lesion formation and progression. Glia. 65, 1900–1913.
Scheld, M., et al., 2016. Neurodegeneration triggers peripheral immune cell recruitment into the forebrain. J. Neurosci. 36, 1410–1415.
Schmierer, K., et al., 2018. Quantifying multiple sclerosis pathology in post mortem spinal cord using MRI. Neuroimage. 182, 251–258.
Siffrin, V., et al., 2010. In vivo imaging of partially reversible th17 cell-induced neuronal dysfunction in the course of encephalomyelitis. Immunity. 33, 424–436.
Silver, N.C., et al., 2001. Quantitative contrast-enhanced magnetic resonance imaging to evaluate blood-brain barrier integrity in multiple sclerosis: a preliminary study. Mult. Scler. 7, 75–82.
Thone, J., et al., 2012. Modulation of autoimmune demyelination by laquinimod via induction of brain-derived neurotrophic factor. Am. J. Pathol. 180, 267–274.
Vollmer, T.L., et al., 2014. A randomized placebo-controlled phase III trial of oral laquinimod for multiple sclerosis. J. Neurol. 261, 773–783.
Wegner, C., et al., 2010. Laquinimod interferes with migratory capacity of T cells and reduces IL-17 levels, inflammatory demyelination and acute axonal damage in mice with experimental autoimmune encephalomyelitis. J. Neuroimmunol. 227, 133–143.
Yang, J.S., et al., 2004. Laquinimod (ABR-215062) suppresses the development of experimental autoimmune encephalomyelitis, modulates the Th1/Th2 balance and induces the Th3 cytokine TGF-beta in Lewis rats. J. Neuroimmunol. 156, 3–9.
Zeis, T., et al., 2008. Normal-appearing white matter in multiple sclerosis is in a subtle balance between inflammation and neuroprotection. Brain. 131, 288–303.
Zinnhardt, B., et al., 2019. Molecular imaging of immune cell dynamics during De- and remyelination in the Cuprizone model of multiple sclerosis by [(18)F]DPA-714 PET and MRI. Theranostics. 9, 1523–1537.
Zou, L.P., et al., 2002. Suppression of experimental autoimmune neuritis by ABR-215062 is associated with altered Th1/Th2 balance and inhibited migration of inflammatory cells into the peripheral nerve tissue. Neuropharmacology. 42, 731–739.